nature climate change

LETTERS

PUBLISHED ONLINE: 4 MAY 2014 | DOI: 10.1038/NCLIMATE2223

# Evolution of land surface air temperature trend

Fei Ji[1,2,3], Zhaohua Wu[3,4]*, Jianping Huang[1,2] and Eric P. Chassignet[3,4]

**The global climate has been experiencing significant warming at an unprecedented pace in the past century[1,2]. This warming is spatially and temporally non-uniform, and one needs to understand its evolution to better evaluate its potential societal and economic impact. Here, the evolution of global land surface air temperature trend in the past century is diagnosed using the spatial–temporally multidimensional ensemble empirical mode decomposition method[3]. We find that the noticeable warming (>0.5 K) started sporadically over the global land and accelerated until around 1980. Both the warming rate and spatial structure have changed little since. The fastest warming in recent decades (>0.4 K per decade) occurred in northern mid-latitudes. From a zonal average perspective, noticeable warming (>0.2 K since 1900) first took place in the subtropical and subpolar regions of the Northern Hemisphere, followed by subtropical warming in the Southern Hemisphere. The two bands of warming in the Northern Hemisphere expanded from 1950 to 1985 and merged to cover the entire Northern Hemisphere.**

In the past two decades, a large body of studies have examined surface air temperature variability and change over the past 160 years on global and regional scales and the resulting social and economic impacts[1,2,4,5]. However, many of these studies focused on averaged warming over that time span using traditional statistical methods, such as straight line fitting, which can extract warming only at a constant rate. As warming on different spatial scales is not uniform over time, such time-unvarying change may not effectively reveal the true nature of climate variability and change. To address this problem, a diagnosis of the evolution of warming on different spatial–temporal scales is necessary.

Here, we focus on how the land surface air temperature trend has evolved since 1900. Traditionally, the shape of a trend is determined a priori, for example, a time-unvarying linear trend or a time-varying exponential trend. Often, little justification is given for why a particular shape of functional form should be used, and the traditional trend lacks the capability of reflecting the hidden nonlinear and nonstationary nature of a time series. Here we adopt a logically consistent definition of trend provided by a previous study[6], that is, a trend of a time series is an intrinsically fitted monotonic function or a function in which there can be at most one extremum within a given data span. This definition requires any identifiable oscillatory components contained in this time span to be removed. Also, an intrinsic trend should require no a priori functional form and can vary with time.

The method we use to separate spatial–temporally varying trend and spatially non-uniform variability of different timescales is the multidimensional ensemble empirical mode decomposition (MEEMD; ref. 3), a method based on ensemble empirical mode decomposition (EEMD; refs 7–9) for time series analysis. In MEEMD, a time series at a grid point $x(t)$ is decomposed using EEMD in terms of adaptively obtained, amplitude–frequency modulated oscillatory components $C_j$ $(j=1,2,\ldots,n)$ and a residual $R_n$, a curve either monotonic or containing only one extremum from which no additional oscillatory components can be extracted:

$$x(t)=\sum_{j=1}^{n} C_j(t)+R_n(t)$$

Examples of such decomposition can be found in Supplementary Figs 2 and 4. As demonstrated in the Supplementary Information and previous studies[6,10], the extracted trend ($R_n$) follows no a priori shape and varies with time after the intrinsic variability of multidecadal and shorter timescales is removed. This trend also has low sensitivity to the extension (addition) of new data. This property guarantees that the physical interpretation within specified time intervals does not change with the addition of new data, consistent with a physical constraint that the subsequent evolution of a physical system cannot alter the reality that has already happened.

For multidimensional spatial–temporal data, we piece together similar timescale components of data series from all grids to form a temporal evolution of the spatially coherent structure of that timescale. This is the essence of MEEMD, with more details introduced in the Supplementary Information and ref. 3. Clearly, MEEMD is a temporally and spatially local method, in contrast to popular domain-dependent methods (for example, empirical orthogonal function analysis), for analysing spatial–temporal climate data. It is anticipated that the temporal and spatial locality provides a better chance for the trend to identify the underlying physical information of data (see Supplementary Information for more discussion). Both EEMD and MEEMD have been widely applied in climate research[10–20].

The data used here are the monthly land surface air temperature from the Climatic Research Unit, University of East Anglia, for the period January 1901 to December 2009, with a horizontal resolution of $0.5^\circ \times 0.5^\circ$ (ref. 21). As we are interested in centennial scale global land warming, the data span adopted for the trend in this study is from 1901 to 2009, with the variability of multidecadal and shorter timescales removed.

Owing to the time-varying nature of the trend defined above, the averaged warming rate (slope) of trend over a given time interval cannot reflect well how the trend has evolved. To overcome this deficiency, here we diagnose the value increment of the EEMD trend at a given time from the reference time of 1901, that is, $\mathrm{Trend}_{\mathrm{EEMD}}(t)=R_n(t)-R_n(1901)$, representing accumulated warming from 1901. This definition also facilitates the comparison of EEMD trend with the corresponding linear trend. The spatial evolution of the accumulated warming by a given time is shown in Fig. 1. Before 1950, noticeable accumulated

[1]College of Atmospheric Sciences, Lanzhou University, Lanzhou 730000, China, [2]Key Laboratory for Semi-Arid Climate Change of the Ministry of Education, College of Atmospheric Sciences, Lanzhou University, Lanzhou 730000, China, [3]Center for Ocean–Atmospheric Prediction Studies, Florida State University, Tallahassee, Florida 32306-2741, USA, [4]Department of Earth, Ocean and Atmospheric Science, Florida State University, Tallahassee, Florida 32306-4520, USA. *e-mail: zwu@fsu.edu

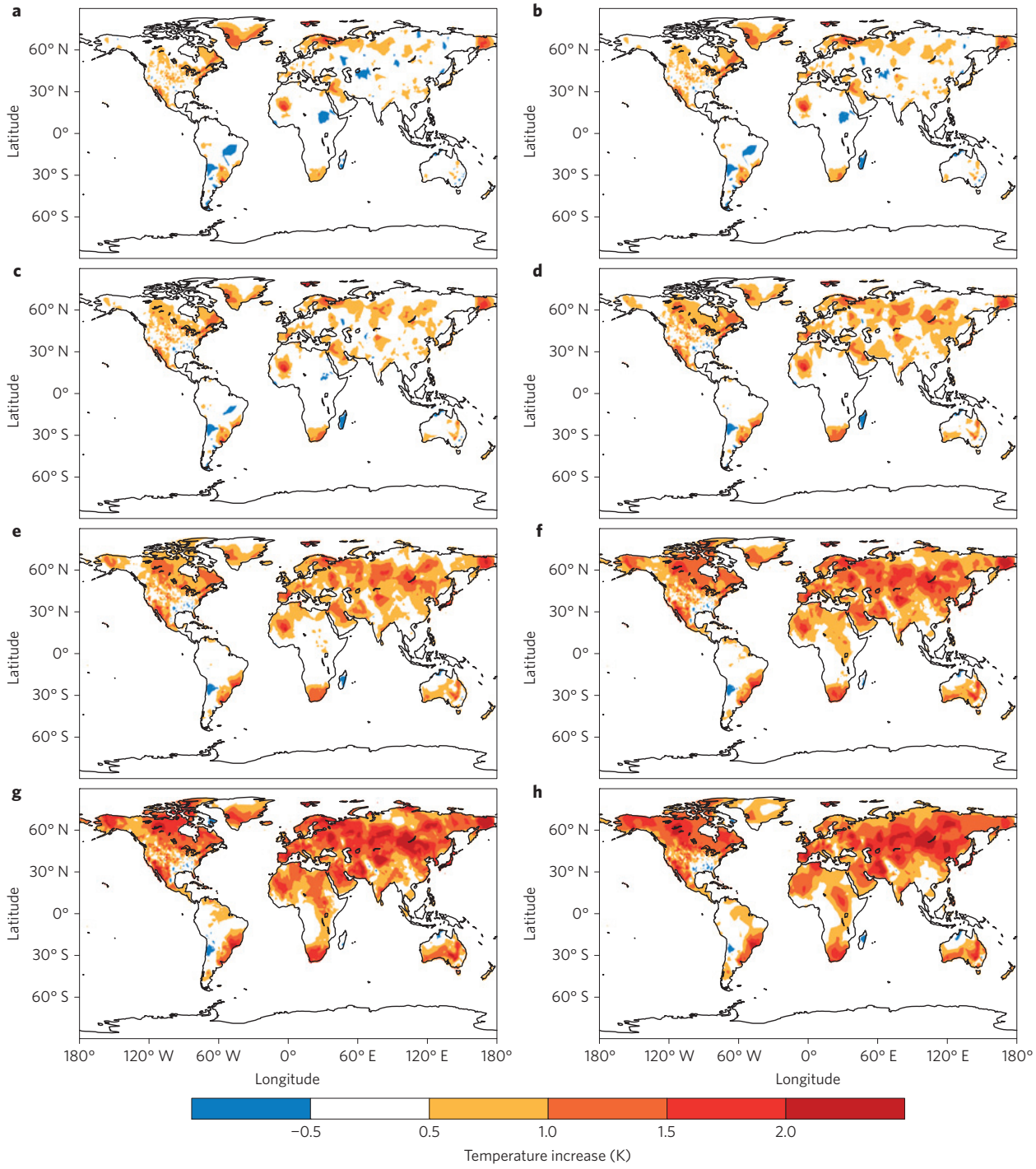


**Figure 1 | Spatial evolution of the ensemble empirical mode decomposition trend of global land surface air temperature. a–g**, Ensemble empirical mode decomposition trends ending in 1950, 1960, 1970, 1980, 1990, 2000 and 2009, respectively. **h**, The spatial structure of temperature increase based on time-unvarying linear trend over the whole data domain from 1901 to 2009.

warming (>0.5 K) or cooling (<−0.5 K) seemed to be sporadically distributed in space, mainly along subtropical bands around 30° S and 30° N and in the subpolar region around 60° N. (The statistical significance against various null hypotheses is presented in the Supplementary Information.) The subtropical bands coincide with the downward branches of Hadley cells. The other noticeable warming region appeared in western Africa near the southern edge of the Sahara Desert. All these regions are arid or semiarid. The earlier sporadic warming has been expanding since 1950. By 1990, the warming regions had expanded across almost all of the northern mid-latitudes. The warmest regions in the Northern Hemisphere do not correspond to the original two bands near 30° N or 60° N; rather, they are in between, that is, located in mid-latitude semiarid regions. The amplitude and spatial patterns of the statistically significant EEMD trend from 1901 to 2009 are slightly different from those of the linear trend over the same period. However, the evolution of the warming pattern cannot be revealed by the linear trend (Fig. 1h).

As the trends obtained are time-varying, their corresponding warming/cooling rates, which can be determined by calculating temporal derivatives of trends, are also temporally and spatially

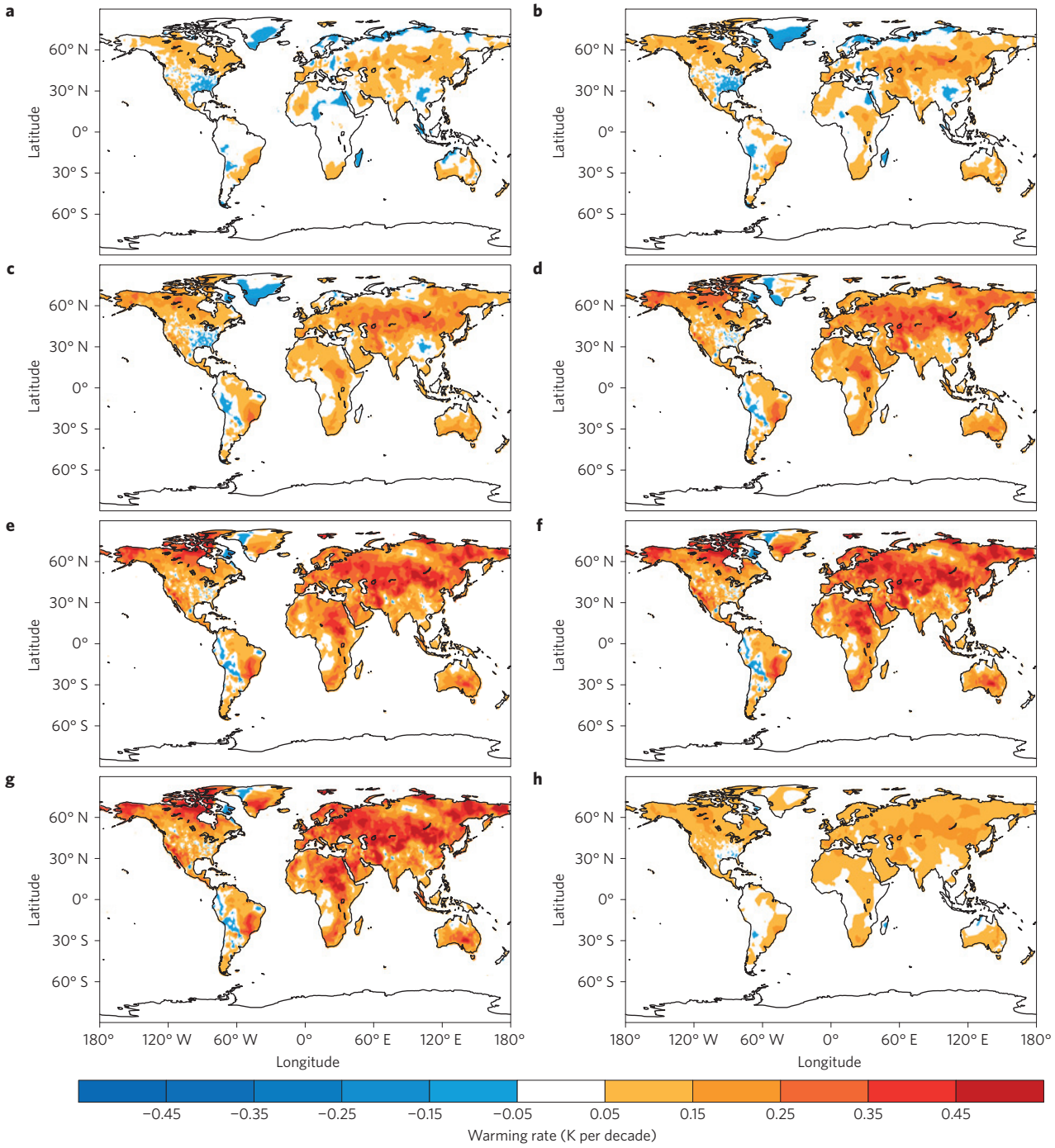


**Figure 2 | Warming rate of global land surface air temperature. a–g**, The instantaneous warming rate of the secular trend in 1950, 1960, 1970, 1980, 1990, 2000 and 2009, respectively. **h**, The spatial structure of the warming rate based on the time-unvarying linear trend over the whole data domain from 1901 to 2009.

local quantities. The warming and cooling rates are shown in Fig. 2. Before 1950, there were both moderate warming and weak cooling regions. The cooling regions shrank and most of them turned into warming regions with an accelerated pace of warming over the next three decades. By 1980, except for the weak cooling in the northern tip of Greenland and in the vicinity of the Andes, almost all the global land had been warming. The warming rates over the global land have changed little since. The strongest warming occurred in the northern mid-latitudes. The spatial structure of the warming rate in later decades resembles that obtained from straight line fitting over the whole temporal domain (Fig. 2h). However, the later warming is much stronger than that determined by the method of straight line fitting.

The zonally averaged trend (over only the land area) is plotted (Fig. 3) so that the main features of the spatial–temporal evolution of the warming can be more evident. To eliminate the noisy pattern caused by spatially sporadic warming, we have applied a running mean over a 5° band in the meridional direction. The zonally averaged warming indeed had a three-band structure (Fig. 3). The noticeable zonally averaged warming (>0.2 K since 1900) first took place in the subtropical and subpolar regions of the Northern Hemisphere, followed by the subtropical warming in

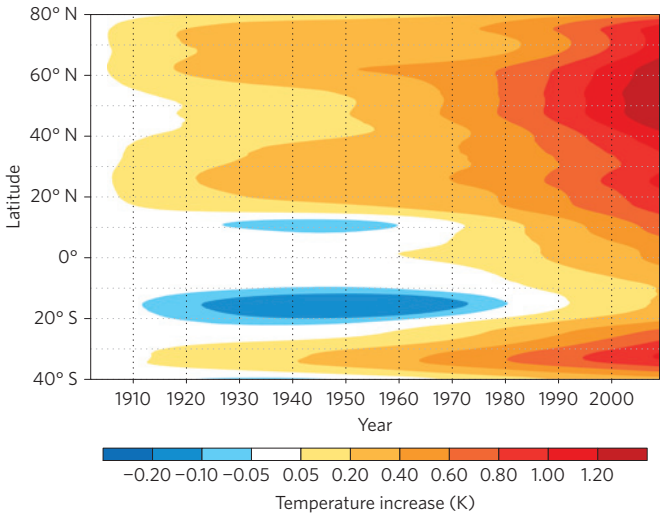


**Figure 3 | Evolution of the zonally averaged trend of surface air temperature.** Note that colour intervals are uneven.

the Southern Hemisphere. In the Northern Hemisphere, this noticeable warming emerged in the northern subtropical and subpolar regions around 1920. The amplitude of the warming grew slowly for both bands, but the latitudinal scope of warming expanded towards mid-latitude during the next three decades, and the 0.2 K lines of these two bands joined by around 1955. From 1955 onwards, the warming accelerated at all latitudes. The greatest warming region in recent decades in the Northern Hemisphere was between the original high-latitude band and the subtropical band. However, these two bands can still be identified by the tongue-like extensions of the contours towards the left-hand side at about 26° N, 62° N and 75° N.

In the Southern Hemisphere, the zonally averaged warming greater than 0.2 K in the subtropical band lagged that of the Northern Hemisphere and was relatively narrow in meridional width. It seems that the poleward warming expansion in the Southern Hemisphere is not as dominant as that of its Northern Hemispheric counterpart, a phenomenon that is possibly related to less land coverage in the Southern Hemisphere mid-latitudes.

It is noted that the above evolution characteristics of the land surface air temperature trend of centennial and longer timescales cannot be revealed by analysing only the later data (for example, 1950 onwards), for the multidecadal variability cannot be separated well from the trend of the later (shorter) data using any analysis method. There is also not enough evidence to argue that the extracted varying trend contains all the anthropogenic effect, for it has been demonstrated that multidecadal variability of land surface air temperature can be caused by natural or anthropogenic forcing of different timescales[10,22–26]. However, the slow-varying nature of the trend seems to be consistent with the slowly increasing carbon dioxide in the atmosphere.

At present, we do not have explanations for why the global land surface trend has evolved as shown in Figs 2 and 3. The relatively earlier warming in the subtropical regions suggests that the warming may be tied to changes in atmospheric circulations, which is consistent with the results of recent studies of the relation between global warming and changes in Hadley cells[27–29]. However, the greatest warming so far associated with (either linear or EEMD) trends occurs in the arid and semiarid regions of the mid-latitude Northern Hemisphere, implying the small heat capacity of the arid and semi-arid regions may also have played a role[30]. The important physical reasons for why the warming trend evolves in this way remain to be investigated.

Received 14 January 2014; accepted 31 March 2014; published online 4 May 2014

## References


1. IPCC *Climate Change 2007: The Physical Science Basis* (eds Soloman, S. *et. al*) (Cambridge Univ. Press, 2007).
2. IPCC *Climate Change 2013: The Physical Science Basis* (eds Stocker, T. F. *et. al*) (Cambridge Univ. Press, 2013).
3. Wu, Z., Huang, N. E. & Chen, X. The multi-dimensional ensemble empirical mode decomposition method. *Adv. Adapt. Data Anal.* **1,** 339–372 (2009).
4. Hansen, J., Ruedy, R., Sato, M. & Lo, K. Global surface temperature change. *Rev. Geophys.* **48,** RG4004 (2010).
5. Lawrimore, J. H. *et al.* An overview of the global historical climatology network monthly mean temperature data set, version 3. *J. Geophys. Res.* **116,** D19121 (2011).
6. Wu, Z., Huang, N. E., Long, S. R. & Peng, C-K. On the trend, detrending and variability of nonlinear and non-stationary time series. *Proc. Natl Acad. Sci. USA* **104,** 14889–14894 (2007).
7. Huang, N. E. *et al.* The empirical mode decomposition method and the Hilbert spectrum for non-stationary time series analysis. *Proc. R. Soc. Lond. A.* **454,** 903–995 (1998).
8. Huang, N. E. & Wu, Z. A review on Hilbert–Huang transform: The method and its applications on geophysical studies. *Rev. Geophys.* **46,** RG2006 (2008).
9. Wu, Z. & Huang, N. E. Ensemble empirical mode decomposition: A noise-assisted data analysis method. *Adv. Atmos. Sci.* **1,** 1–41 (2009).
10. Wu, Z., Huang, N. E., Wallace, J. M., Smoliak, B. V. & Chen, X. On the time-varying trend in global-mean surface temperature. *Clim. Dynam.* **37,** 759–773 (2011).
11. Franzke, C. Multi-scale analysis of teleconnection indices: Climate noise and nonlinear trends analysis. *Nonlinear Proc. Geoph.* **16,** 65–76 (2009).
12. Ruzmaikin, A. & Feynman, J. Search for climate trends in satellite data. *Adv. Adapt. Data Anal.* **1,** 667–679 (2009).
13. Qian, C., Wu, Z., Fu, C. B. & Zhou, T. J. On multi-timescale variability of temperature in China in modulated annual cycle reference frame. *Adv. Atmos. Sci.* **27,** 1169–1182 (2010).
14. Vecchio, A. & Carbone, V. Amplitude–frequency fluctuations of the seasonal cycle, temperature anomalies, and long-range persistence of climate records. *Phys. Rev. E.* **82,** 066101 (2010).
15. Franzke, C. & Woollings, T. On the persistence and predictability properties of North Atlantic climate variability. *J. Clim.* **24,** 466–472 (2011).
16. Fu, C., Qian, C. & Wu, Z. Projection of global mean surface air temperature changes in next 40 years: Uncertainties of climate models and an alternative approach. *Sci. China Earth Sci.* **54,** 1400–1406 (2011).
17. Hu, Z. Z., Huang, B., Kinter, J. L. III, Wu, Z. & Kumar, A. Connection of the stratospheric QBO with global atmospheric general circulation and tropical SST Part II: Interdecadal variations. *Clim. Dynam.* **38,** 25–43 (2012).
18. Huang, B. *et al.* Influences of subtropical air–sea interaction on the multidecadal AMOC variability in the NCEP climate forecast system. *Clim. Dynam.* **39,** 631–555 (2012).
19. Zhu, J., Huang, B. & Wu, Z. The role of ocean dynamics in the interaction between the Atlantic meridional and equatorial modes. *J. Clim.* **25,** 3583–3598 (2012).
20. Misra, V., Li, H., Wu, Z. H. & DiNapoli, S. Global seasonal climate predictability in a two tiered forecast system: Part I: Boreal summer and fall seasons. *Clim. Dynam.* **42,** 1425–1448 (2014).
21. Mitchell, T. D. & Jones, P. D. An improved method of constructing a database of monthly climate observations and associated high-resolution grids. *Int. J. Climatol.* **25,** 693–712 (2005).
22. Semenov, V. A. *et al.* The impact of North Atlantic–Arctic multidecadal variability on Northern Hemisphere surface air temperature. *J. Clim.* **23,** 5668–5677 (2010).
23. DelSole, T., Tippett, M. K. & Shukla, J. A significant component of unforced multidecadal variability in the recent acceleration of global warming. *J. Clim.* **24,** 909–926 (2011).
24. Booth, B. B., Dunstone, N. J., Halloran, P. R., Andrews, T. & Bellouin, N. Aerosols implicated as a prime driver of twentieth-century North Atlantic climate variability. *Nature* **484,** 228–232 (2012).
25. Tung, K. K. & Zhou, J. Using data to attribute episodes of warming and cooling in instrumental records. *Proc. Natl Acad. Sci. USA* **110,** 2058–2063 (2013).
26. Zhang, R. *et al.* Have aerosols caused the observed Atlantic multidecadal variability? *J. Atmos. Sci.* **70,** 1135–1144 (2013).
27. Hudson, R. D., Andrade, M. F., Follette, M. B. & Frolov, A. D. The total ozone field separated into meteorological regimes–Part II: Northern

Hemisphere mid-latitude total ozone trends. *Atmos. Chem. Phys.* **6,** 5183–5191 (2006).
28. Hu, Y. & Fu, Q. Observed poleward expansion of the Hadley circulation since 1979. *Atmos. Chem. Phys.* **7,** 5229–5236 (2007).
29. Seidel, D. J., Fu, Q., RanDel, W. J. & Reichler, T. J. Widening of the tropical belt in a changing climate. *Nature Geosci.* **1,** 21–24 (2008).
30. Huang, J., Guan, X. & Ji, F. Enhanced cold-season warming in semi-arid regions. *Atmos. Chem. Phys.* **12,** 5391–5398 (2012).

## Acknowledgements

This work was supported by the National Basic Research Program of China 2012CB955301 (F.J. and J.H.) as well as the US National Science Foundation program AGS-1139479 (Z.W. and F.J.).

## Author contributions

All authors contributed to shaping up the ideas and writing the paper. The analyses were carried out by F.J. and Z.W., with various analysis methods designed by Z.W., F.J. and Z.W. are co-first authors.

## Additional information

Supplementary information is available in the online version of the paper. Reprints and permissions information is available online at www.nature.com/reprints. Correspondence and requests for materials should be addressed to Z.W.

## Competing financial interests

The authors declare no competing financial interests.

nature climate change

SUPPLEMENTARY INFORMATION

DOI: 10.1038/NCLIMATE2223

# Evolution of land surface air temperature trend

**Evolution of land surface air temperature trend**

Fei Ji[1,2,4], Zhaohua Wu[3,4], Jianping Huang[1,2], and Eric P. Chassignet[3,4]

1. College of Atmospheric Sciences
Lanzhou University, Lanzhou, China

2. Key Laboratory for Semi-Arid Climate Change of the Ministry of Education
College of Atmospheric Sciences
Lanzhou University, Lanzhou, China

3. Department of Earth, Ocean and Atmospheric Science
Florida State University
Tallahassee, Florida, USA

4. Center for Ocean-Atmospheric Prediction Studies
Florida State University
Tallahassee, Florida, USA

Submitted to *Nature Climate Change*
March 2014

Corresponding author: Dr. Zhaohua Wu
Department of Earth, Ocean and Atmospheric Science
Center for Ocean-Atmospheric Prediction Studies
Florida State University
Tallahassee, Florida
zwu@fsu.edu

Here we introduce the multi-dimensional ensemble empirical mode decomposition (MEEMD) method and the statistical significant test method associated with MEEMD. The introduction contains moderate details of these methods and describes the advantages of MEEMD in diagnosing climate system evolution.

## 1. The Multi-dimensional Ensemble Empirical Mode Decomposition

The main method used in this study is the multidimensional ensemble empirical mode decomposition[1] (MEEMD), which was developed based on the empirical mode decomposition[2,3] (EMD) and ensemble empirical mode decomposition[4] (EEMD). EMD is a one-dimensional data analysis method that is adaptive, has high locality, and can theirby handle the nonlinear and nonstationary nature of data. EEMD adds robustness to the EMD decomposition when data is perturbed by noise, guaranteeing that the physical interpretation of the decomposition result is not sensitive to the noise inevitablly contained in real data. The robustness of EEMD provides the foundation for the development of MEEMD for analysing multidimensional spatial-temporal data. Although EMD and EEMD have been cited thousands of times in scientific and engineering literatures, they are still not standard methods in climate research. Here we introduce EMD, EEMD, and MEEMD methods, with an emphasis on the rationality behind the development of each.

### *a. The Empirical Mode Decomposition*

The original purpose of the development of EMD was to set up appropriate conditions for using the Hilbert transform (HT) to calculate instantaneous frequency[2,3,5]. It is now well known that the instantaneous frequency of a given time series obtained via HT has physical meaning only when that time series is a mono-component, i.e., the time series can be expressed in terms of a product of an amplitude function and a carrier with the former having much slower variation than the latter. The very early development of EMD focused on decomposing any given time series in terms of mono-components of different time scales. The combination of EMD and HT provides a novel time-frequency-

energy representation for any given time series and is now widely called Hilbert-Huang Transform (HHT).

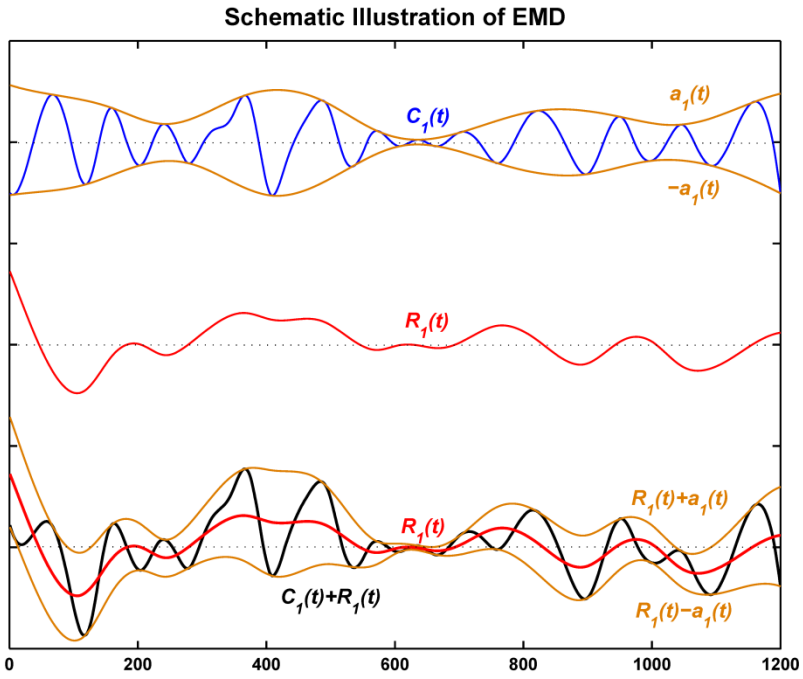


**Figure 1**: **The intuition behind EMD**. The blue line $C_1$ is a pure oscillatory component (mono-component) with its amplitude $a_1(t)$ being given as the brown line at the top; the red line is the background slower varying component $R_1$; and the black line is the sum of $R_1$ and $C_1$. Among the bottom group curves, the brown lines are $R_1(t) + a_1(t)$ and $R_1(t) - a_1(t)$, respectively.

EMD is intuitively simple, as shown in Fig. 1: Suppose there is a time series composed of a mono-component ($C_1$) and a relatively slower varying component ($R_1$). The mono-component $C_1$ can be expressed as the product of an amplitude function $a_1(t)$ and a pure oscillatory function with changing instantaneous frequency $\omega_1(t)$. For this mono-component, $a_1(t)$ is its upper envelope and $-a_1(t)$ is its lower envelope. As illustrated in Fig. 1, the time series $C_1+R_1$ are confined within two curves $R_1(t)+a_1(t)$ and $R_1(t)-a_1(t)$ and, therefore, these two curves serve as upper and lower envelopes of the inputted time series, respectively. An interesting feature that deserves attention is that $R_1(t)+a_1(t)$ appears to be a smooth curve that passes through all the maxima of the signal and $R_1(t)-a_1(t)$ the smooth curve that connects all the minima. If the example is considered in a reversed way: for any given $C_1+R_1$, by finding the upper and lower

envelopes that smoothly connect all the maxima and all the minima of $C_1$+$R_1$, one can define approximately $R_1$ and separate the riding wave $C_1$ from slower varying component background $R_1$.

The actual algorithm of EMD, in which the extracted mono-component is obtained through a refining process called "sifting", is a bit more complicated: For an input time series *x(t)*, (1) set $x_1(t) = x(t)$; (2) find maxima and minima of $x_1(t)$; (3) obtain upper envelope $e_u(t)$ and lower envelope $e_l(t)$ by using cubic splines to connect maxima and minima, respectively; (4) find the local mean $m(t) = [e_u(t) + e_l(t)]/2$ ; and (5) determine whether *m(t)* is close enough to zero (equivalent to the symmetric of the upper and lower envelopes with respect to zero line) at anywhere under a given criterion. If yes, stop sifting; otherwise, set $x_1(t) = x(t) - m(t)$ and repeat steps 2 to 5. In this way we obtain the first riding wave component (formally called intrinsic mode function [IMF]). By subtracting this riding wave component from *x(t)*, we obtain a remainder. If the remainder still contains oscillatory components, we again repeat steps 2 to 5 but with new $x_1(t)$ being the remainder. A complete EMD process ends when the remainder is a monotonic function or a curve contains at most one extremum at which no more oscillatory component can be defined. In this way, we decompose $x_1(t)$, i.e.,

$$x(t) = \sum_{j=1}^{n} C_j(t) + R_n(t) = \mathrm{Re}\left[\sum_{j=1}^{n} a_j(t)\, e^{i\int \omega_j(t)\,dt}\right] + R_n \quad , \tag{1}$$

where $\mathrm{Re}[\bullet]$ represents the real part of "$\bullet$", and $a_j(t)$ and $\omega_j(t)$ are instantaneous amplitude and frequency of $j^{\text{th}}$ IMF, respectively.

While EMD is intuitively simple, it does possess many wonderful properties: (1) The decomposition is sparse and appears to be a dyadic filter bank in its normal parameter regime[6-8] so the decomposition is highly effective; (2) when EMD is applied to pulse (delta-function-like) signals, EMD performs like a bank of spline wavelet of different orders[8,9]; (3) when EMD is applied to noise of different colors, the EMD components of different timescales have the same Fourier spectrum[6-8] after rescaling the

components in both frequency and amplitude; and (4) all but the first EMD components of noise have a Gaussian distribution[7]. These naturally emerged intriguing and hidden simplicities not only connect EMD with earlier widely used decomposition methods, such as Fourier spectrum-based filtering and wavelet decomposition, but also highlight the unique characteristics that other methods do not possess.

*b. The Ensemble Empirical Mode Decomposition*

Since EMD uses the extrema information to separate the riding "natural" wave and its reference, changes in extrema locations and values could lead to significantly different results, which makes the extracted "natural" wave sometimes appear bizarre and very sensitive to any noise, since noise can alter the local extrema both in location and value. One of the consequences of this characteristic of EMD is that the analysis of two almost identical data series (e.g, the records collected by two almost identical observations of the same phenomenon) using EMD may result in significantly different decompositions, potentially leading to totally different physical interpretations. This lack of robustness and the "physical uniqueness" essentially caused many complaints about the ineffectiveness of EMD.

To overcome this drawback, the ensemble empirical mode decomposition (EEMD), a noise assisted data analysis method, was developed[3,4]. The method is based on the understandings of characteristics of noise using EMD as mentioned in section 1a, i.e., EMD is effectively a dyadic filter bank for noise[6,7]. EEMD consists of the following steps: (1) add a white noise series to the targeted data $x(t)$; (2) decompose the data with added white noise into IMFs; (3) repeat step 1 and step 2 again and again, but with different white noise series added each time; and (4) obtain the (ensemble) means of corresponding IMFs of the decompositions as the final result. The effect of the added white noise in EEMD is to provide a dyadic filtering reference frame in the time-frequency space; therefore, the added noise collates the portion of the signal of comparable scale in one IMF, significantly reducing the chance of mode mixing and leading to the stability of decomposition. As the EMD is a temporal domain analysis method, the white noise is averaged out with a sufficient number of trials. In this sense,

the added noise mimics multiple observations of a phenomenon recorded by a single observation and serves as a "catalyst" in the decomposition that leads to stable and more physically interpretable results. An example of EEMD decomposition of the global annual mean land surface air temperature is displayed in Fig. 2.

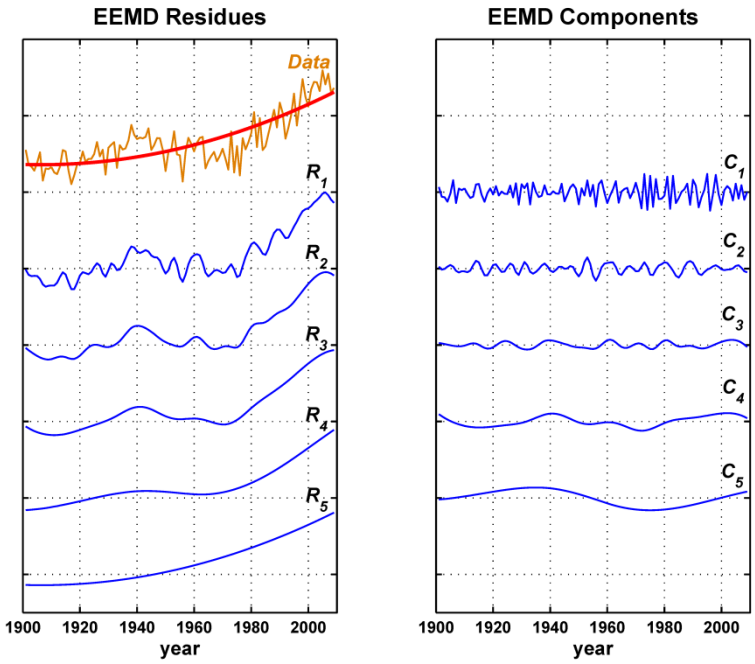


**Figure 2**: **EEMD decomposition of the global annual mean land surface air temperature.** In the left panel, the original data (brown line) and successive remainders ($R_j$) after an additional EEMD component ($C_j$) are extracted, i.e., $R_j=R_{j-1}-C_j$ for $j>1$. The red line is the EEMD trend. In the right panel, each line represents an EEMD component ($C_j$), from high frequency to low frequency.

As argued in previous studies[10,11], the locality of data analysis provides a necessary condition to effectively isolate physical information of data. If the information extracted from the data does reflect the physical processes operating at a given time, then the information should be temporally local quantity and the corresponding physical interpretation within specified time intervals should also not change with the addition of new data, for the subsequent evolution of a physical system cannot alter the reality that has already happened. For EMD, temporal locality is well preserved if a fixed number of sifting is given[7]. This locality is inherited by EEMD, as tested extensively in previous studies[7,11]. Here we presented an example displayed in Fig. 3, in which the different spans of the same data are decomposed. Evidently, the closeness of the corresponding

components over the overlapped span is very high and the locality of the decomposition is well preserved.

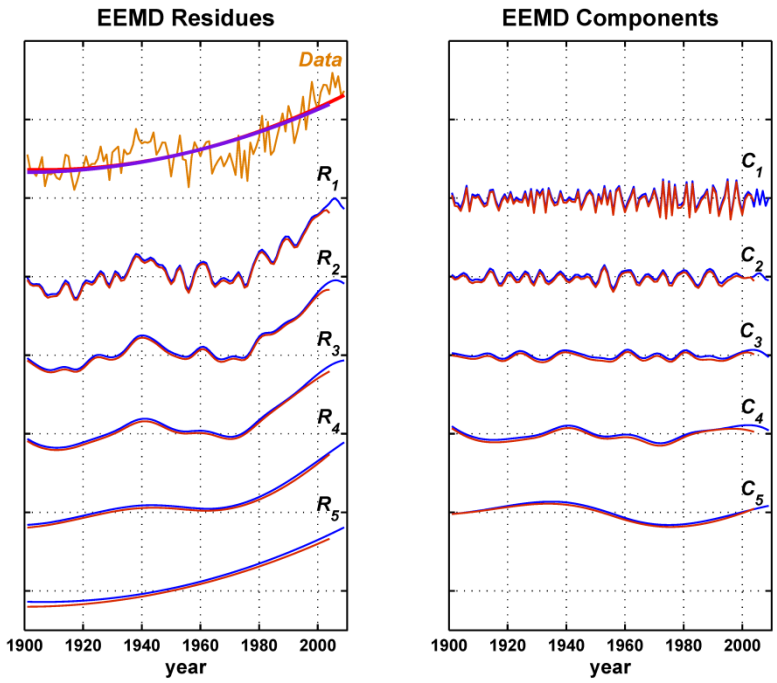


**Figure 3**: **Temporal locality of EEMD decomposition.** The brown and blue lines are identical to those displayed in Fig. 2. The red lines are from EEMD decomposition of the data of a shortened temporal span. For easier identification, the red lines are intentionally downshifted by a small margin.

In addition to the well-preserved locality, EEMD also possesses two exciting properties that help address the problems of non-stationarity and excessive harmonics in data analysis: (1) EMD/EEMD analysis makes the stationarity assumption irrelevant, for the analysis results are not affected by the data far away. The temporal locality of an analysis method automatically bypasses the stationarity assumption which is often applied over the global domain of data; (2) when EMD/EEMD is applied, the harmonic problem is gone. In EMD/EEMD, the nonlinearity is expressed by the modulations of amplitude and frequency (scale), as illustrated by simple nonlinear oscillators[2,12]. Since EMD/EEMD approximates the envelope of the riding wave using only extrema information, the waveform between two neighboring maxima (minima) is well preserved, therefore, the harmonics become unnecessary.

*c. The Multidimensional Ensemble Empirical Mode Decomposition*

One-dimensional data analysis methods (such as many time series analysis methods and EMD/EEMD described above) have limitations in extracting spatial-temporally coherent information contained in multidimensional data. In climate science, various matrix-based eigenvalue-eigenfunction calculation methods have been widely used, e.g., empirical orthogonal function (EOF) analysis[13-16] and its variations. In such methods, spatial structures and temporal evolutions are often assumed separable and the spatial structures remain unchanged throughout the climate system evolution. Such an assumption is certainly questionable from both physical and mathematical perspectives[17-19]. An easy validation of this assumption can be carried out by testing the sensitivity of the obtained static spatial structures and corresponding temporal variations to the change of temporal domain of the inputted data. High sensitivity implies the lack of the validity of the assumption. A similar argument can be applied to the spatial sensitivity. There are other methods, such as principal oscillation pattern analysis[20,21] or footprinting methods[22] that can handle either spatial locality or temporal locality, but not both. It should be noted that most of these methods contain implicit assumption of the stationarity of data.

The MEEMD was developed to handle both spatial locality and temporal locality issues[1]. There are two types of MEEMD: one for the decomposition of spatial data such as images and the other for temporal-spatial data such as gridded climate data. It is the latter type of MEEMD that we use in this study. As mentioned earlier, EEMD is highly temporally local and has low sensitivity to noise. Since the method is based on identifying extrema locations, the signal propagation from one spatial location to its neighboring area (as indicated by the different temporal locations of extrema) can be pinned down. Using this property, we can identify the small variations of different timescales of a climate variable at neighboring areas, as demonstrated in Fig. 4. Evidently, the small original data differences of various timescales are well captured: the sharp, short-duration difference of the original data at around 1940 (the blue line having larger change than the red line) is identified in $C_1$; and the relatively longer duration difference in the original data (the blue line staying above the red line) from 1980 to 2000 is

reflected in $C_3$ and $C_4$. The slight shifts of the troughs of $C_3$ for these three locations around 1990 are also identifiable.

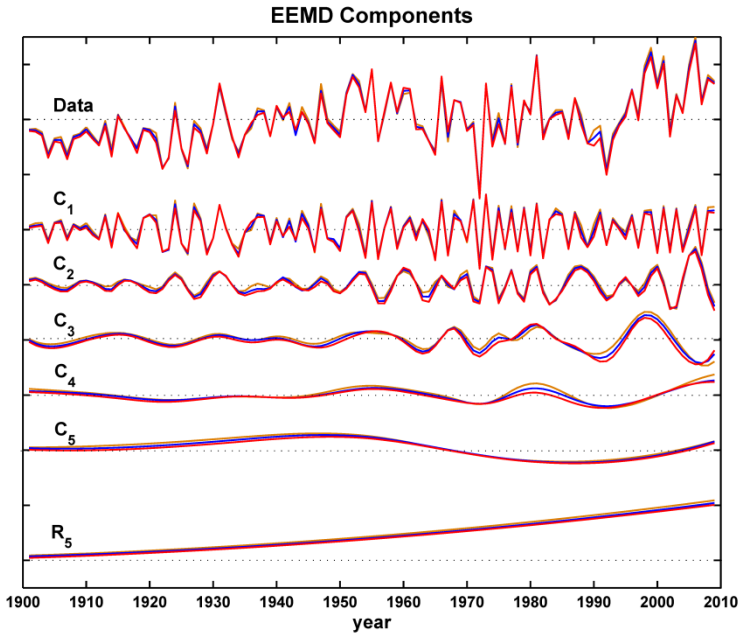


**Figure 4**: **Spatial coherence of EEMD decomposition.** Surface air temperatures at three neighboring grids are decomposed using EEMD. Brown lines correspond to grid point (70.25°W, 55.25°N), blue lines grid point (71.25°W, 55.25°N), and red lines grid point (72.25°W, 55.25°N). The top group of lines is the original surface air temperature data and the following groups are the components of different naturally separated timescales.

The spatial coherence displayed in Fig. 4 provides the basic idea of MEEMD algorithm for the decomposition of multidimensional spatial-temporal climate data: (1) decompose the time series of a climate variable at any grid using EEMD; and (2) piece together the $j^{th}$ components ($C_j$) or $j^{th}$ remainders ($R_j$) from all grids to form the evolution of the $j^{th}$ components or $j^{th}$ remainders. An example of MEEMD decomposition is given in Fig. 5. From this simple procedure, it is quite evident that MEEMD is absolutely spatially local, for the decomposition of data at one grid is completely independent of the data at other grids. Since all the components are additive, a component of a broader timescale may combine the neighboring components (e.g., $C_j+C_{j+1}$). To some degree, EEMD serves as a natural filter that can handle both the static and propagating (expanding) signals of a climate variable of a naturally determined timescale. If there is a

spatially static pattern, MEEMD identifies this pattern, as the middle panel of Fig. 5 displays; if there is a systematic propagation of signal, MEEMD also extracts this signature, as the fourth (from the top) panel displays.

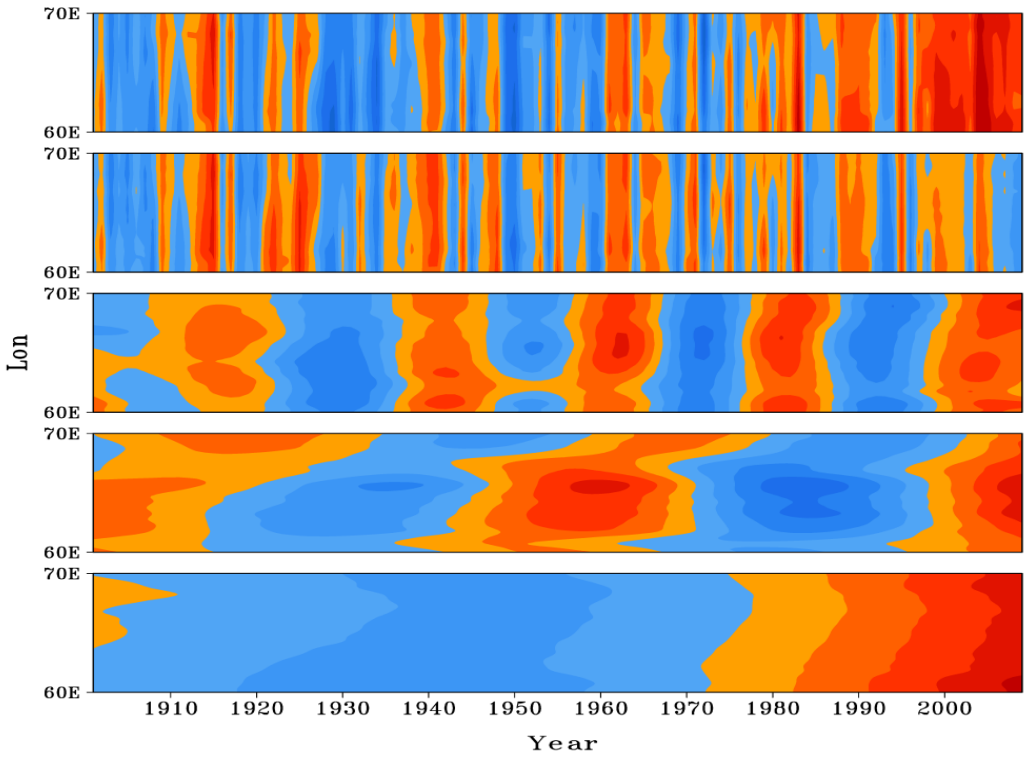


**Figure 5**: **MEEMD decomposition of land surface air temperature.** The decomposition of land surface air temperature (with mean value at each grid subtracted) at 45.25°N is displayed in the top panel; the second panel (from the top) is the sum of $C_1$, $C_2$ and $C_3$; the third panel C4; the fourth panel C5, and the bottom panel R5. Color schemes for different panels are different (not shown).

The adaptiveness and locality of MEEMD give unique advantages to MEEMD over many other methods in analyzing temporal-spatial multidimensional data. On one hand, MEEMD does not invoke any significant mathematical constraints such as shape functions (e.g., trigonometric functions in Fourier transform and mother wavelet in wavelet analysis), and its basic ingredient is the "natural" wave forms obtained adaptively from data themselves. The inclusion of amplitude and temporal-spatial scale modulations in a component allows for the reflection of the physical world complications caused by nonlinear interactions and nonstationary external forcing. On the other hand,

the temporal locality of EMD satisfies a fundamental physical principle: If components extracted from the data do reflect the physical processes operating at a given time, these components should be temporally local quantities and the corresponding physical interpretation within specified time intervals should also not change with the addition of new data, for the subsequent evolution of a physical system cannot alter the reality that has already happened. The spatial locality allows MEEMD to identify the propagating or expanding signals. The combination of the spatial and temporal locality of MEEMD provides advantages when examining both the static climate mode and changing spatial structures of climate variability, thereby giving a more powerful method to diagnose climate system evolution.

*d. Some Technical Details of EMD/EEMD/MEEMD in This Study*

As discussed in section 1a, EMD involves a sifting process to obtain an oscillatory mono-component. In this process, a stoppage criterion is needed to determine the symmetry of the upper and lower envelopes of that mono-component with respect to the zero line. In Huang et al.[2], a Cauchy type condition that is a sort of energy integration over the global temporal domain is adopted. EMD decomposition of data with this condition is quite sensitive to the data domain as well as the noise contained in the data and can compromise the locality of EMD. To improve the locality, Wu and Huang[4] proposed a fixed-number sifting stoppage criterion. As shown in Wu and Huang[4] and Wu et al.[8], this new stoppage criterion can satisfy the Cauchy type condition to a high accuracy. With this new criterion, EMD also serves as a more accurate dyadic filter and the locality of EMD is dramatically improved. More details can be found in Appendix A of Wu and Huang[4] and Wu et al.[8].

Another issue in EMD decomposition is the data end treatment. The determination of envelopes using spline (or other polynomials) requires boundary conditions of a natural spline if past and future data is unknown. There is no real solution to this problem, for a good extension of data requires an accurate prediction of remote future data, especially when low-frequency components and the trend of data are pursued. As we know, for any physical system, prediction of the slowly varying components of

data to the near future is usually more accurate than the prediction of fast-varying components. With this in mind, we adopted a linear extrapolation approach to obtain the envelope end values using the nearest two interior maxima (minima) to an end for the upper (lower) envelope rather than to predict actual data. Additional correction is also included when the actual data are located outside such determined envelopes. More details of this end treatment and its good performance can be found in Appendix B of Wu and Huang[8].

In EEMD calculation, the noise added to data has an amplitude of 0.2 standard deviations of the corresponding data and the ensemble number is 400.

A MATLAB EMD/EEMD package with the above stoppage criterion and end treatment is downloadable at http://rcada.ncu.edu.tw/research1.htm. Although some of our calculations in this study use a Fortran counterpart, the results should be repeatable with the MATLAB package albeit with a slower computational speed.

## 2. Statistical Significant Test of MEEMD Trend

The statistical significance test of a quantity of a given data involves three issues: (1) the null hypothesis adopted about the data; (2) the determination of the probability density function (PDF) of a quantity consistent with the null hypothesis; and (3) whether the quantity of the data has a small probability to occur based on the PDF. If the probability of the quantity to occur is indeed small, the null hypothesis is rejected and the quantity is considered statistically significant. In such a sense, the statistical significance is highly sensitive to the adopted null hypothesis and making a reasonable null hypothesis about the data becomes a key issue.

In climate sciences, two widely used null hypotheses about climate data are white noise and red noise. Any climate data contain white noise (corresponding to stochastic changes) so that a white noise null hypothesis is the most intuitive. However, when a climate quantity is a response rather than the stochastic forcing itself, often a red noise process is adopted[23]. The redness of the process is related to the long-term memory (inertial) of the climate system. In a thermodynamic stochastic model in which the

temperature response is studied, the inertial of the climate system is the effective heat content of the climate system[23]. Due to the spatial heterogeneity of the thermodynamic properties of the climate system, the memory is different over different regions. Figure 6 plots the auto-correlation of one temporal interval lag (lag-1 auto-correlation) of the yearly mean surface air temperature over the global land. Clearly, the spatial heterogeneity is quite high.

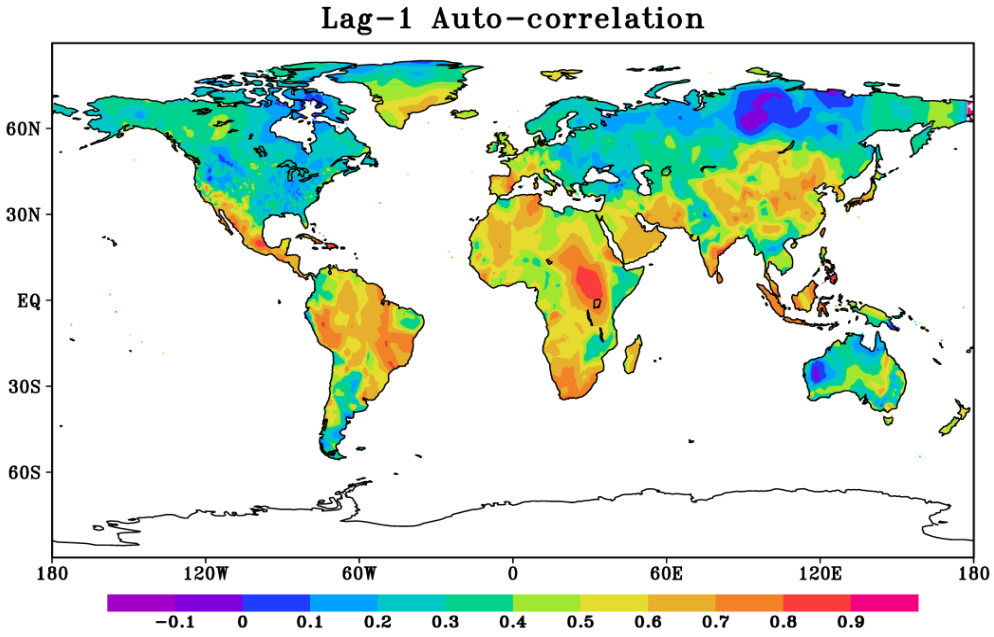


**Figure 6**: **Lag-1 auto-correlation of land surface air temperature.** The values of the lag-1 auto-correlation are indicated by the colorbar at the bottom of the figure.

The statistical significance test of linear trends of climate series against a red noise null hypothesis has been widely adopted in climate studies[24-26]. For nonlinear non-stationary components extracted using EMD, various test methods have been proposed. The very first one was an analytical expression of statistical significance based on the characteristics of white noise decomposed by EMD[6,7], which was applied to various climatic indices[7]. Franzke[27] extended the above method to test statistical significance of EMD components against a red noise null hypothesis. Recently, Wu et al.[11] proposed an alternative method for determining the significance of the multidecadal component of a climate series resulting from EEMD against a null hypothesis of red noise. However, these approaches were not designed for testing the significance of the secular trend

obtained using EEMD. In addition, the earlier methods did not consider the data end effect on the secular trend.

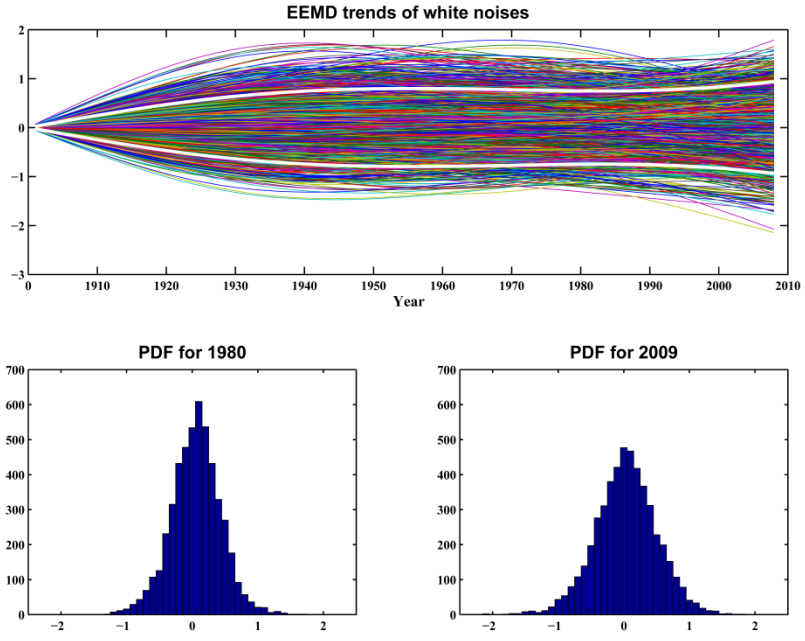


**Figure 7**: **EEMD trends of white noise series and their distributions.** The upper panel plots EEMD trends of 5000 white noise series (thin lines of different colors); the lower left and right panels plot the histograms of EEMD trend values for locations 1980 and 2009, respectively. Two bold white lines are two-standard-deviation spread lines. It is noted that the time axis of white noise series is from 1901 to 2009 (109 data points) so as to align with the temporal domain of the land surface air temperature analyzed.

*a. Statistical significance test method*

In this study, we propose an approach to determine the statistical significance of the secular trends of temporal-spatial multi-dimensional climate data based on a Monte Carlo method. In this new approach, we generate 5000 samples of red noise series of the same temporal data length (109) and lag-1 auto-correlation as the yearly mean land surface air temperature at each grid. We apply EEMD to each series to determine its secular trend and obtain the empirical PDF of the values of EEMD trends at any temporal location (the increment/decrement of the secular trend value from its starting value, see the main text for the definition). The EEMD trends at any temporal location and their PDFs of two selected temporal locations are plotted in Fig. 7 for a zero lag-1 auto-correlation case (white noise series). Clearly, the EEMD trends of noise series have a

larger spread in later period, especially near the data end, partially caused by data end treatment of EMD/EEMD. The PDFs are approximately normally distributed. The trend spread depends on the value of lag-1 auto-correlation. When the noise is getting redder (larger lag-1 auto-correlation), the corresponding spreads become wider, as plotted in Fig. 8.

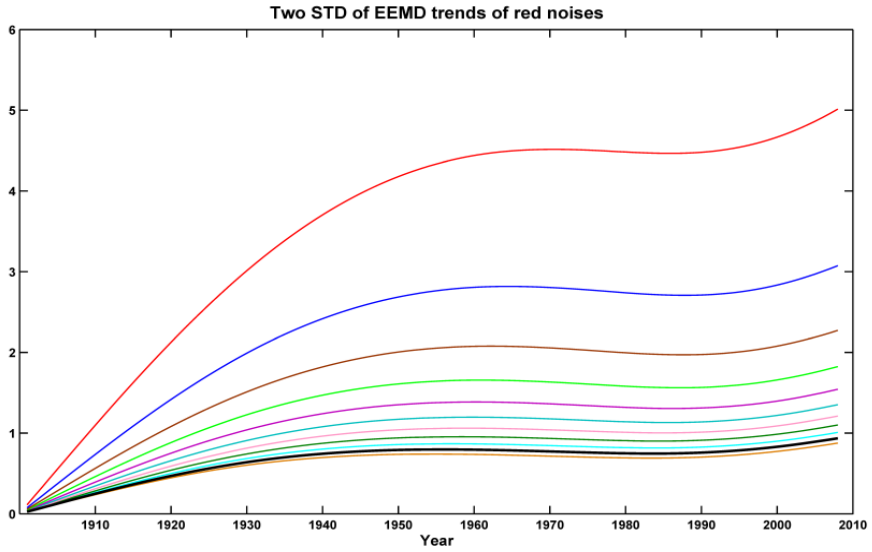


**Figure 8**: **Two-standard-deviation curves of EEMD trends of red noise series of different lag-1 auto-correlation.** The curves from the bottom to the top correspond to lag-1 auto-correlations of -0.1, 0, 0.1, 0.2, 0.3, 0.4, 0.5, 0.6, 0.7, 0.8, and 0.9, respectively. The bold black line is identical to the upper bold white curve in Fig. 7.

To determine whether an EEMD trend of land surface air temperature at a given temporal-spatial location is statistically significant, we (1) divide the EEMD trend of that spatial location by the standard deviation of the corresponding temperature data; (2) find the two-standard-deviation spread value of the trends of the red noise series having the same lag-1 auto-correlation as the corresponding temperature data; and (3) check whether the trend value is beyond the two-standard-deviation level (slightly larger than 95% of confidence) of the noise EEMD trend PDF at the given temporal location. If it is, the EEMD trend is considered statistically significant. Clearly, for the same value of EEMD trends at different locations, whether the value is statistically significant depends on both spatial and temporal locations.

*b. Statistical significance test without consideration of spatial coherence*

The result of the independent application of the designed statistical significance test method to the EEMD trends of individual land surface air temperature series is presented in Fig. 9. Compared with Fig. 1 of the main paper, the regions of warming/cooling that pass the statistical significance test are noticeably smaller, although subtropical spots of significant warming in both hemispheres and northern high latitude spots are still identifiable. In later decades, the warming in low latitudes fails the statistical significance test due to larger long-term memories, as illustrated in Fig. 6.

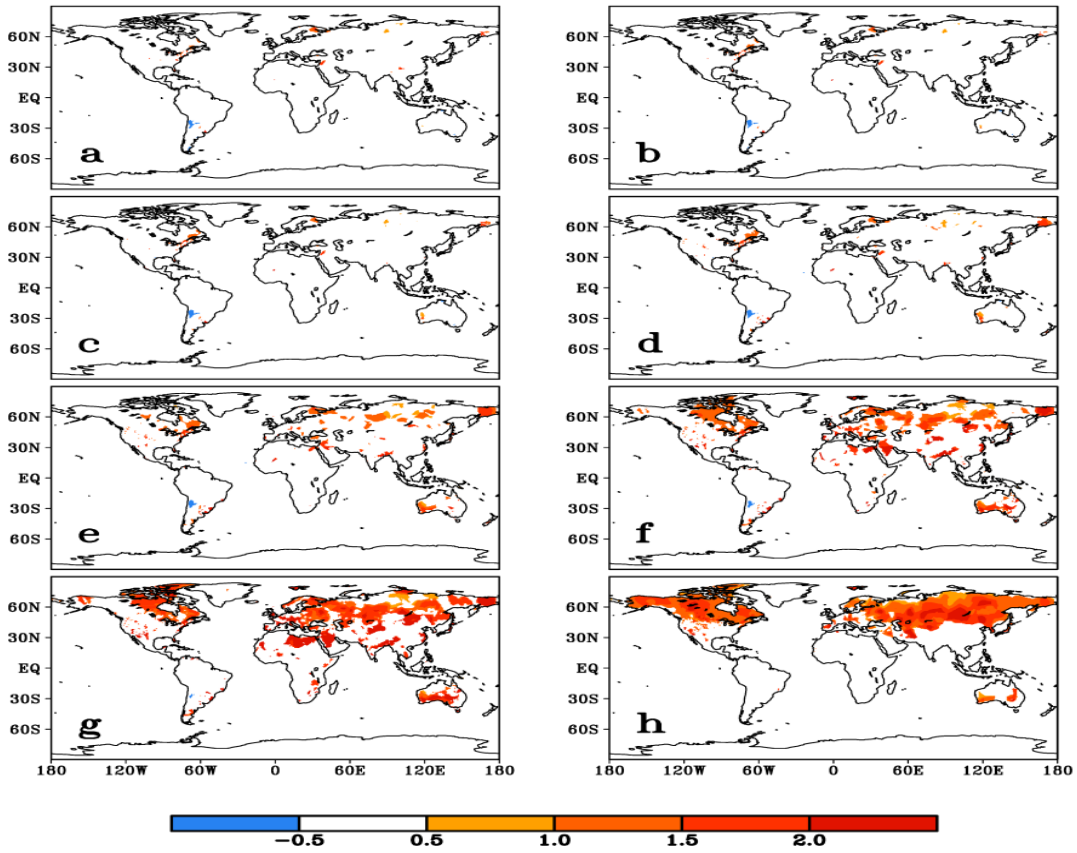


**Figure 9: Statistically significant EEMD trend of global land surface air temperature without considering spatial coherence.** Panels ***a*** to ***g*** represent statistically significant EEMD trends ending at 1950, 1960, 1970, 1980, 1990, 2000 and 2009, respectively. Panel ***h*** displays the spatial structure of temperature increase based on time-unvarying linear trend over the whole data domain from 1901 to 2009. The underlying colorbar gives the temperature increase, with a unit Kelvin (K).

*c. Statistical significance test with consideration of spatial coherence*

In previous studies[24-28], many climatic indices studied are regional or globally averaged climate variables. When each of these indices is treated, spatial coherence is taken for granted and the averaged spatial domain is implicitly assumed uniform. Under such an implicit assumption, a statistical significance test is carried out following a selected white/red null hypothesis on a climatic index. As clearly shown in Fig. 6, the heterogeneity of memory makes it hard to select configurations of domains for spatial averaging. In addition, the different spatial coherence itself casts doubts on the appropriateness of an *a priori* null hypothesis. These caveats make it more challenging to design an appropriate statistical significance test method.

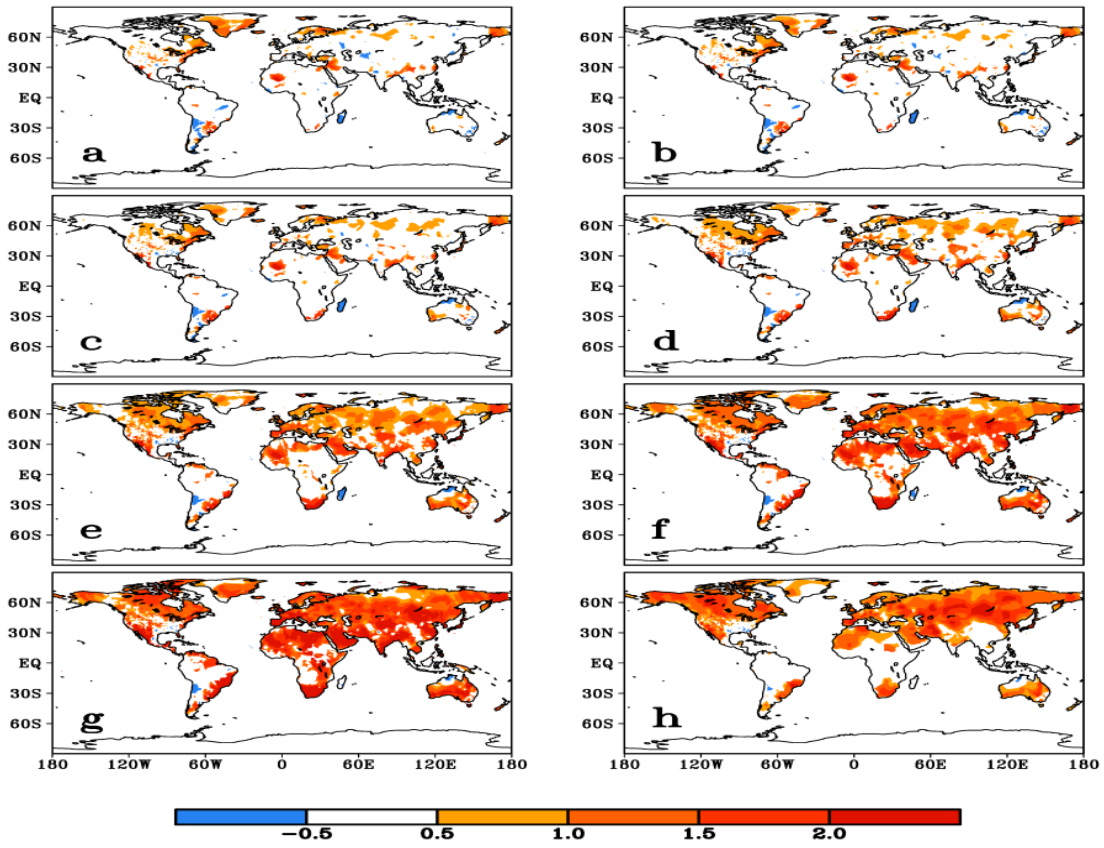


**Figure 10: Statistically significant EEMD trend of global land surface air temperature with consideration of spatial coherence.** Same as Fig. 9 but for the four-grid-point averaged red noise null hypothesis.

As described in previous sections, the EEMD trends of land surface air temperature presented in Fig. 1 of the main paper are calculated grid by grid. When the spatially coherent (e.g., region averaged) trends are considered, to be consistent, the trends of red noise used in the null hypothesis for different grids over the same region must be averaged as well. Since the red noise realizations in the Monte Carlo method for different grids are independent of each other, based on the central limit theorem, the spread is inversely proportional to the square root of the number of grids averaged for neighboring grids of almost identical lag-1 auto-correlation. Under this consideration, the spatially coherent trends are much easier to pass the same statistically significant level than the case without consideration of spatial coherence. Examples of four-grid-point averaged and nine-grid-point averaged cases are presented in Figs. 10 and 11, respectively.

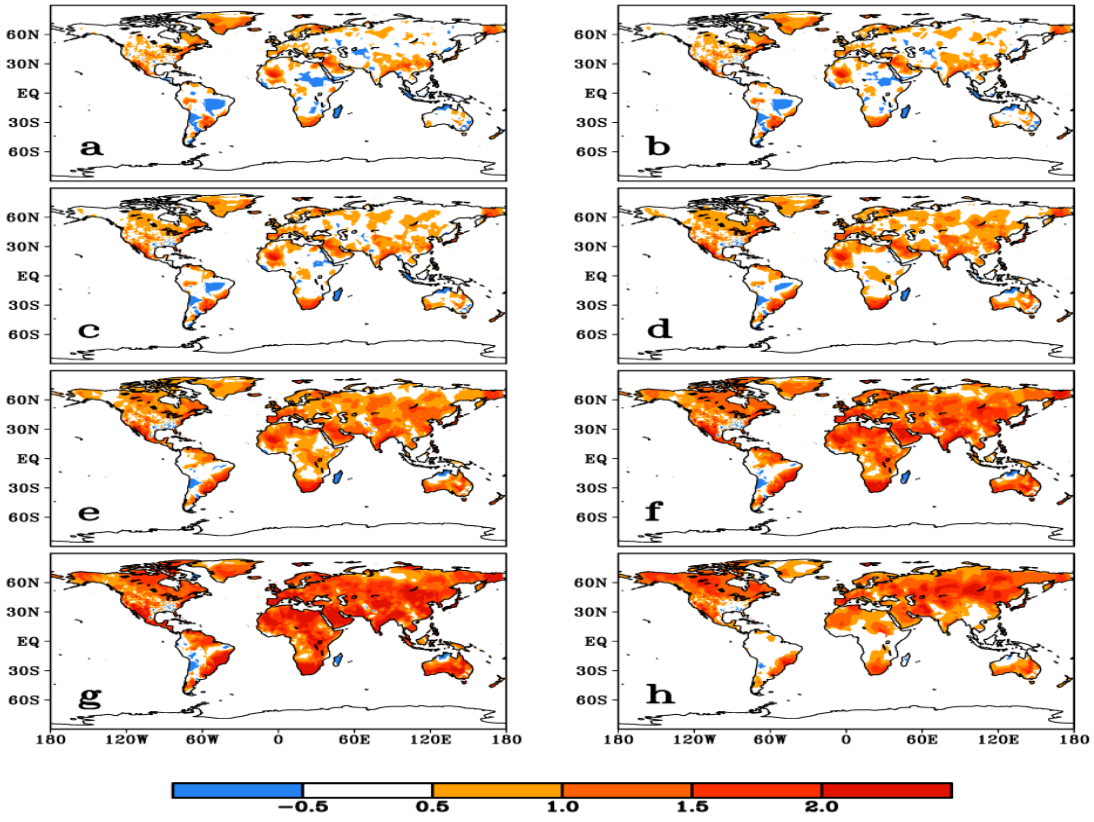


**Figure 11: Statistically significant EEMD trend of global land surface air temperature with the consideration of spatial coherence.** Same as Fig. 9 but for the nine-grid-point averaged red noise null hypothesis.

As shown in Figs. 9 to 11, an inclusion of only a small spatial coherence can lead to significantly enlarged regions that pass the statistical significance against the same null hypothesis. This sensitivity illustrates the limitation of the statistical significance test approach.

## References


(1) Wu, Z., Huang, N. E. & Chen, X. The multi-dimensional ensemble empirical mode decomposition method. *Adv. Adapt. Data Anal*. **1,** 339–372 (2009).

(2) Huang, N. E. *et al.* The empirical mode decomposition method and the Hilbert spectrum for non-stationary time series analysis. *Proc. R. Soc. Lond. A.* **454,** 903–995 (1998).

(3) Huang, N. E. & Wu, Z. A review on Hilbert–Huang transform: the method and its applications on geophysical studies. *Rev. Geophys.* **46,** RG2006 (2008).

(4) Wu, Z. & Huang, N. E. Ensemble empirical mode decomposition: a noise-assisted data analysis method. *Adv. Atmos. Sci.* **1,** 1–41 (2009).

(5) Huang, N. E. *et al.* On instantaneous frequency. *Adv. Adapt. Data Anal*. **1,** 177–229 (2009).

(6) Flandrin, P., Rilling, G. & Gonçalvès, P. Empirical mode decomposition as a filter bank. *IEEE Signal Processing Lett.* **11,** 112–114 (2004).

(7) Wu, Z. & Huang, N. E. A study of the characteristics of white noise using the empirical mode decomposition method. *Proc. R. Soc. Lond. A.* **460,** 1597–1611 (2004).

(8) Wu, Z. & Huang, N. E. On the Filtering Properties of the Empirical Mode Decomposition. *Adv. Adapt. Data Anal*. **2,** 397–414 (2010).

(9) Flandrin, P. & Goncalves, P. Empirical mode decompositions as data-driven wavelet-like expansions. *Int. J. Wavelets Multiresolut. Inf. Process.* **2,** 477–496 (2004).

(10) Wu, Z., Huang, N. E. & Chen, X. Some considerations on physical analysis of data. *Adv. Adapt. Data Anal*. **3,** 95–113 (2011).

(11) Wu, Z., Huang, N. E., Wallace, J. M., Smoliak, B. V. & Chen, X. On the time-varying trend in global-mean surface temperature. *Clim. Dynam.* **37,** 759–773 (2011).

(12) Huang, N. E. Shen, Z. & Long, S. R. A new view of nonlinear water wave–the Hilbert spectrum. *Ann. Rev. Fluid Mech.* **31,** 417–457 (1999).

(13) Lorenz, E. N. Empirical orthogonal functions and statistical weather prediction. *Sci. rep. no. 1, statist.* (1956).

(14) Wallace, J. M. Empirical orthogonal representation of time series in the frequency domain. part II: application to the study of tropical wave disturbances. *J. Appl. Meteor.* **11,** 893–900 (1972).

(15) Wallace, J. M. & Dickinson, R. E. Empirical orthogonal representation of time series in the frequency domain. part I: theoretical considerations. *J. Appl. Meteor*. **11,** 887–892 (1972).

(16) Thompson, D. W. J. & Wallace, J. M. The arctic oscillation signature in the wintertime geopotential height and temperature fields. *Geophys. Res. Lett*. **25,** 1297–1300 (1998).

(17) Dommenget, D. & Latif, M. A cautionary note on the interpretation of EOFs. *J. Climate*. **15,** 216–225 (2002).

(18) Hannachi, A., Jolliffe, I. T. & Stephenson, D. B. Empirical orthogonal functions and related techniques in atmospheric science: A review. *Int. J. Climatol*. **27,** 1119–1152 (2007).

(19) Monahan, A. H., Fyfe, J. C., Ambaum, M. H. P., Stephenson, D. B. & North, G. R. Empirical orthogonal functions: The medium is the message. *J. Climate*. **22,** 6501–6514 (2009).

(20) Hasselmann, K. PIPs and POPs: The reduction of complex dynamical systems using principal interaction and oscillation patterns. *J. Geophys. Res.* **93,** 11015–11021 (1988).

(21) von Storch, H. & Xu, J. Principal oscillation pattern analysis of the 30-to 60-day oscillation in the tropical troposphere. *Clim. Dynam.* **4,** 175–190 (1990).

(22) Vimont, D. J., Battisti, D. S. & Hirst, A. C. Footprinting: A seasonal connection between the tropics and mid-latitudes. *Geophys. Res. Lett.* **28,** 3923–3926 (2001).

(23) Hasselmann, K. Stochastic climate models part I. Theory. *Tellus*. **28,** 473–485 (1976).

(24) Santer, B. D. *et al.* Statistical significance of trends and trend differences in layer-average atmospheric temperature time series. *J. Geophys. Res.* **105,** 7337–7356 (2000).

(25) Steig, E. J. *et al.* Warming of the Antarctic ice-sheet surface since the 1957 International Geophysical Year. *Nature*. **457,** 459–462 (2009).

(26) Bromwich, D. H. *et al.* Tropospheric clouds in Antarctica. *Reviews of Geophysics*. **50,** RG1004 (2012).

(27) Franzke, C. Multi-scale analysis of teleconnection indices: Climate noise and nonlinear trends analysis. *Nonlin. Processes Geophys.* **16,** 65–76 (2009).

(28) Wunsch, C. The interpretation of short climate records, with comments on the North Atlantic and Southern Oscillations. *Bulletin of the American Meteorological Society*. **80,** 245–255 (1999).